Published in final edited form as:
NMR Biomed. 2011 November ; 24(9): 1119–1128. doi:10.1002/nbm.1667.

MRI evaluation of axonal reorganization after bone marrow stromal cell treatment of traumatic brain injury

Quan Jiang[a,b,*], **Changsheng Qu**[c], **Michael Chopp**[a,b], **Guang Liang Ding**[a], **Siamak P. Nejad-Davarani**[a], **Joseph A. Helpern**[e], **Jens H. Jensen**[d,f], **Zheng Gang Zhang**[a,b], **Lian Li**[a], **Mei Lu**[g], **David Kaplan**[h], **Jiani Hu**[i], **Yimin Shen**[i], **Zhifeng Kou**[i], **Qingjiang Li**[a], **Shiyang Wang**[a,b], and **Asim Mahmood**[c]

[a]Department of Neurology, Henry Ford Health System, Detroit, MI, USA

[b]Department of Physics, Oakland University, Rochester, MI, USA

[c]Department of Neurosurgery, Henry Ford Health System, Detroit, MI, USA

[d]Department of Radiology, New York University School of Medicine, New York, NY, USA

[e]Department of Radiology and Radiological Science, Medical University of South Carolina, Charleston, South Carolina

[f]Department of Physiology and Neuroscience, New York University School of Medicine, New York, NY, USA

[g]Department of Biostatistics and Research Epidemiology, Henry Ford Health System, Detroit, MI, USA

[h]Department of Biomedical Engineering, Tufts University, Medford, MA, USA

[i]Harper Hospital, MR Center, Detroit, MI, USA

Abstract

We treated traumatic brain injury (TBI) with human bone marrow stromal cells (hMSCs) and evaluated the effect of treatment on white matter reorganization using MRI. We subjected male Wistar rats ($n = 17$) to controlled cortical impact and either withheld treatment (controls; $n = 9$) or inserted collagen scaffolds containing hMSCs ($n = 8$). Six weeks later, the rats were sacrificed and MRI revealed selective migration of grafted neural progenitor cells towards the white matter reorganized boundary of the TBI-induced lesion. Histology confirmed that the white matter had been reorganized, associated with increased fractional anisotropy (FA; $p < 0.01$) in the recovery regions relative to the injured core region in both treated and control groups. Treatment with hMSCs increased FA in the recovery regions, lowered T_2 in the core region, decreased lesion volume and improved functional recovery relative to untreated controls. Immunoreactive staining showed axonal projections emanating from neurons and extruding from the corpus callosum into the ipsilateral cortex at the boundary of the lesion. Fiber tracking (FT) maps derived from diffusion tensor imaging confirmed the immunohistological data and provided information on axonal rewiring. The apparent kurtosis coefficient (AKC) detected additional axonal remodeling regions with crossing axons, confirmed by immunohistological staining, compared with FA. Our data demonstrate that AKC, FA, FTand T_2 can be used to evaluate treatment-induced white matter recovery, which may facilitate restorative therapy in patients with TBI.

[*]Correspondence to: Q. Jiang, Henry Ford Hospital, NMR Laboratory, Neurology Department, 2799 West Grand Boulevard, Detroit, MI 48202, USA.

Keywords

MRI; DTI; traumatic brain injury; rat brain

INTRODUCTION

Traumatic brain injury (TBI) is a significant factor in human morbidity. As many as 50 000 Americans die from TBI each year, and an equal number become disabled (1). Treatment has primarily focused on acute therapeutic intervention to reduce cellular damage and brain edema (2); however, currently available techniques cannot repair biostructural damage to the neurons. New strategies designed to enhance functional recovery after TBI and stroke using pharmacological and cell-based neurorestorative techniques have shown promising results in animals, promoting functional recovery and brain remodeling (3,4). The administration of bone marrow stromal cells (MSCs) after TBI in rats improved significantly motor, sensory, modified neurological severity score (mNSS), and learning and memory tests compared with nontreated rats within days to weeks after treatment (3,4).

Therapeutic benefit may depend on the migration and localization of grafted cells within the target tissue (5). Our current understanding of the migration of transplanted cells within the brain has been derived mainly from regional measurements of cell grafts using histological and immunohistological methods (6); however, these techniques do not allow the dynamic assessment of graft migration, and only one measurement can be performed per animal. MRI offers excellent anatomical resolution and specificity, as labeled contrast agents can target specific cells directly (7–9). Several researchers have reported the visualization of magnetically labeled cells in the brain after transplantation (7–9). However, dynamic MRI evaluation of cell migration and distribution has seldom been applied to TBI. In the current study, we used MRI to investigate dynamic changes in labeled cells and white matter reorganization after TBI.

Although a few groups have demonstrated that MRI can detect noninvasively the migration of labeled cells in the brain, we know of no systematic and dynamic study of the effects of cell therapy on brain tissue, such as neuronal remodeling and functional recovery. The functional outcome of TBI cannot be explained by focal pathology alone (10), and diffuse axonal injury (DAI) and reorganization are primary contributors to neurocognitive deficits and recovery, respectively (11–13). The ability to define precisely the extent of axonal injury and recovery immediately after the brain is injured remains a major diagnostic challenge, because these injuries are seldom visible on computed tomography or conventional T_1- and T_2-weighted MRI (14,15). Over the past few years, diffusion tensor MRI (DTI) has been found to have potential benefit in the assessment of DAI after brain injury (11,12) and has often been applied successfully (11–13), suggesting that this method could improve our understanding of brain injury and improve the diagnosis in these patients. DTI has reportedly revealed reduced fractional anisotropy (FA) in major white matter tracts in the central areas of the brain (11,12). The treatment of brain injury with MSCs after stroke promotes axonal remodeling and increases oligodendrocyte formation (remyelination) (16,17). Thus, FA may also be helpful for the assessment of white matter remodeling after TBI. However, when white matter fiber tracts lie across each other, conventional DTI is unable to resolve multiple overlapping fibers and merely shows an overall lowering in FA, because of the assumption of Gaussian diffusion inherent to the tensor model (18–20). Recently, it has been shown that, in brain regions containing fiber crossing, the MR diffusion signal has a significant multimodal structure, in clear disagreement with the conventional tensor model (19,21–23). Solving the orientation distribution function (ODF), which is used to describe the directionality of multimodal diffusion in regions with complex

fiber architecture (22,24), can detect crossing fibers more accurately (21–23); this involves a complex set of *q*-space DTI (*q*-DTI) analysis, including diffusion spectrum imaging (DSI) (21), *q*-ball (22) and persistent angular structure MRI (PASMRI) (23). In addition, diffusional kurtosis has been introduced as a quantitative measure of the degree to which the diffusion displacement probability distribution deviates from a Gaussian form, and MRI diffusional kurtosis imaging (DKI) has been described to measure this quantity (25,26). Indeed, DKI has been shown recently to provide the information necessary to solve the ODF (27), whereas the apparent kurtosis coefficient (AKC) can provide additional information on neural tissue microarchitecture (28). In the current study, we investigated the effects of MSC treatment on the migration and distribution of MSCs and neuronal remodeling using MRI. Our data demonstrated that MRI is capable of noninvasively monitoring cell migration and distribution, as well as brain tissue remodeling, which has the potential to enhance functional recovery.

MATERIALS AND METHODS

All experimental procedures were approved by the Institutional Animal Care and Use Committee and the Institutional Review Board of Henry Ford Hospital.

Cell labeling, and collagen scaffold and human MSC (hMSC) preparation

The hMSCs were provided by Theradigm (Baltimore, MD, USA). Ferumoxide suspension (Feridex IV; Berlex Laboratories, Wayne, NJ, USA), at a concentration of 50 μg/mL was placed in a mixing flask containing serum-free RPM1 1640 medium (Biosource, Camarillo, CA, USA), *N*-2-hydroxyethylpiperazine-*N*′-2-ethanesulfonic acid (HEPES) (25 mM), minimum essential medium (MEM), nonessential amino acids, sodium pyruvate and L-glutamine, and protamine sulfate (American Pharmaceuticals Partner, Schaumburg, IL, USA), at a concentration of 5 μg/mL was added. The ferumoxide and protamine sulfate were mixed for 5–10 min, intermittently shaking the flask by hand. Then, an equal volume of a solution containing ferumoxide–protamine sulfate complexes was added to the cell culture, which was incubated overnight. The labeled hMSCs were suspended in phosphate-buffered saline prior to injection.

Ultrafoam scaffolds made of collagen type I (Davol, RI, USA) were soaked overnight in culture medium consisting of Dulbecco's modified Eagle's medium supplemented with 10% fetal calf serum, 100 U/mL penicillin, 100 μg/mL streptomycin, 0.1 mM nonessential amino acids and 1 ng/mL basic fibroblast growth factor (Life Technologies, Rockville, MD, USA), and then aseptically transferred to a sterile 50-mL centrifuge tube, allowing the scaffold to settle at the bottom of the tube. Following trypsinization, hMSCs were transferred gently into 200 μL of culture medium, and then another 100 μL was applied twice to opposite sides of the scaffold. The scaffold and cell solution were incubated for 30 min in a humidified incubator to facilitate primary cell seeding, after which the centrifuge tubes were placed in a humidified incubator, together with 3 mL of culture medium, and incubated overnight until scaffold implantation.

Animal model and experiment

Wistar rats ($n = 17$), weighing 270–300 g, were injured via controlled cortical impact (29,30) and either left untreated ($n = 9$) or injected with the collagen scaffold plus 3×10^6 hMSCs (31) ($n = 8$). The scaffolds with a three-dimensional lattice can better support cells as a temporary extracellular matrix after transplantation, but do not have a significant effect on the functional outcome when compared with saline injection (31,32). The scaffold was transplanted into the core of the lesion 7 days after TBI. During surgery and hMSC

injection, animals were anesthetized with 3.5% halothane and maintained with 1.0–2.0% halothane in $N_2O : O_2$ (2 : 1).

MRI measurements

MRI measurements were obtained using a 7-T, 20-cm-bore superconducting magnet (Magnex Scientific, Abingdon, Oxford-shire, UK) interfaced with a Bruker console (Billerica, MA, USA). The 12-cm-bore actively shielded gradient coil set is capable of producing magnetic field gradients up to 20 G/cm. A saddle radiofrequency coil was used as the transmitter and a surface coil as the receiver. Stereotaxic ear bars were used to minimize movement during the imaging procedure. Anesthesia was maintained during MRI using a mixture of N_2O (69%), O_2 (30%) and halothane (0.75–1%). The rectal temperature was kept at 37 ± 0.5 °C using a feedback-controlled water bath. A tri-pilot scan of the imaging sequence was used to ensure reproducible positioning of the animal in the magnet for each session. MRI measurements, FA, T_2 and three-dimensional MRI were performed before, 2 days and 1, 2, 3, 4 and 5–6 weeks after TBI. *Ex vivo* DTI was performed on two treated animals 1 day after death, or 6 weeks after TBI.

Measurement of DTI—DTI was measured using the Stejskal–Tanner sequence with two b values (10 and 1200 s/mm^2) in each of six diffusion sensitizing directions, 13 slices, 1-mm slice thickness, 32-mm field of view, 128 × 64 matrix, TR = 1.5 s and TE = 40 ms. Each scan took 3.2 min, and the entire sequence took about 19.2 min.

Measurement of T_2—T_2 was measured using standard two-dimensional Fourier transform multislice multi-echo MRI. Four sets of images (13 slices per set) were obtained using TEs of 20, 40, 60 and 80 ms and TR of 3 s. Images were produced using a 32-mm field of view, 1-mm slice thickness and 128 × 64 image matrix. The entire sequence took about 3.2 min.

High-resolution three-dimensional measurements—Three-dimensional gradient-echo images were obtained with TR = 40 ms, TE = 10 ms, flip angle of 30° and 32 × 32 × 16 mm^3 field of view. The 256 × 192 × 64 voxel matrix was interpolated to 256 × 256 × 64 voxels (0.125 × 0.125 × 0.25 mm^3) for analysis.

Ex vivo q-DTI measurement—q-Ball-based DTI was performed using a pulsed gradient spin-echo sequence with the following parameters: field of view, 32 mm; four signal average, 128 × 128 imaging matrix; 1-mm slice thickness with 16 slices; TR = 1.5 s; TE =38 ms; δ = 12 ms; Δ = 20 ms; 128 diffusion attenuated directions with b = 1500 s/mm^2 for each slice (23); total acquisition time, ~27 h.

Ex vivo DKI measurement—DKI data were acquired using a pulsed gradient spin-echo sequence with the following parameters: field of view, 32 mm; four signal average, 128 × 128 imaging matrix; 1-mm slice thickness with 16 slices; TR = 1.5 s; TE = 50 ms; δ = 18 ms; Δ = 25 ms; 29 diffusion attenuated weighted images with b = 2500, 2000, 1500, 1000 and 500 s/mm^2 for each slice (25,26); total acquisition time, ~31 h.

Histological analysis

Tissue preparation and Prussian blue staining—The brain was rapidly removed after final MRI (6 weeks after TBI) and perfused with heparinized saline. To detect superparamagnetic labeled hMSCs in the brain, sections were stained for iron using Prussian blue. Coronal sections were incubated for 30 min with 2% potassium ferrocyanide (Perl's reagent) in 6% HCl, washed and counterstained with nuclear fast red (9).

Immunohistochemistry—To detect any changes in cerebral white matter, immunohistochemistry was performed on paraffin-embedded coronal sections (6 μm). The axonal fiber tracts were examined using a combination of Nissl and silver stains (Bielshowsky staining) (33). Bielshowsky staining was used to show the axons and Luxol fast blue (34) staining for myelin. For Bielshowsky staining, we placed slides in 20% silver nitrate in the dark, added ammonium hydroxide until the tissues turned brown with a gold background, and then added sodium thiosulfate. Finally, the slides were stained in Luxol fast blue, washed in 95% alcohol and placed in lithium carbonate. Nuclei are colorless, myelin is blue and axons are black.

Functional outcome

The mNSS (35) was determined by observers blind to the treatments at 1 day and 1, 2, 3, 4, 5 and 6 weeks after TBI, and a modified Morris water maze test (36) was performed at 38, 39, 40, 41 and 42 days after TBI.

Data analysis

The FA and fiber tracking (FT) data were analyzed using DTI studio software (37). We analyzed *q*-DTI using Camino (23,38) and estimated AKC from the DKI data using diffusional kurtosis estimator software provided by Drs Jensen and Helpern. T_2 was calculated on a pixel-by-pixel basis (13). The injured lesion was identified in the T_2 maps at different time points after TBI using the threshold T_2 value of the mean + 2 standard deviations from the T_2 value measured in the ipsilateral hemisphere on T_2 maps obtained pre-TBI. The injured core was identified from the injured lesion 6 weeks after TBI. Lesions seen on the T_2 maps were always smaller 6 weeks after TBI compared with 2 days; therefore, the second region of interest (ROI), the recovery area, was identified by subtracting the injured core observed 6 weeks after TBI from the lesion seen on the T_2 maps 2 days after TBI.

Statistics

Observations are presented as the mean ± standard error. To study the regional effect on MRI measurements (injured core *versus* recovery ROIs), double repeated measure analysis of variance (ANOVA) was employed, including the dependent factors of region and time of assessment within a given subject and the independent factor of treatment. To test the effect of treatment on MRI parameters, ANOVA was conducted with the dependent factor of time and the independent factor of treatment. A two-sample *t*-test was performed to test the effect of treatment on MRI measurements.

RESULTS

MRI tracking of labeled cells after TBI

The migration and distribution of hMSCs after TBI in a representative treated rat brain are shown in Fig. 1. No obvious signal hypointensities were detected before hMSC transplantation of MSCs (2 days); however, the same rat exhibited signal hypointensity (representing labeled cells) around the boundary of the TBI core (arrowheads) 9 days after TBI (2 days after implantation). A similar signal hypointensity was observed 1 week after implantation, together with increased hypointense areas in the injured core. By 3–6 weeks after TBI, the core lesion had gradually decreased and the areas of signal hypointensity representing labeled cells merged together, with the labeled cells moving towards the center of the brain along the corpus callosum (arrowheads). The areas of signal hypointensity seen on MRI were not detected in the contralateral hemisphere at any time after transplantation (9 days to 6 weeks). Sections obtained from the same rat 6 weeks after TBI (C–E, D and E

from the boxed areas in C) showed clusters of Prussian blue-stained cells around the boundary of the lesion and corpus callosum (D and E, arrowheads), consistent with the findings on MRI.

In order to confirm that the blue cells were indeed hMSCs and not iron particles that had undergone phagocytosis by microglia or macrophages, we performed double staining with an antibody against human mitochondria and Prussian blue. hMSCs were identified by antibodies against human mitochondria (red cells in Fig. 2A, C; arrows) and iron particles were labeled by Prussian blue (dark black cells in Fig. 2B; arrows). These Prussian blue-labeled hMSCs localized to the boundary region had single nuclei indicated by 4′,6-diamidino-2-phenylindole (A and C, blue) and did not exhibit microglia/macrophage morphology.

Quantitative characterization of white matter reorganization based on MRI parameters

Damaged areas were measured on the T_2 maps in both treated and control groups. The damaged areas in the treated group decreased significantly ($p < 0.05$) by 3–6 weeks when compared with those in the control group.

FA and T_2 were measured in the injured core and recovery area based on relative changes from normal values in the core and recovery ROIs. Figure 3 shows temporal profiles of the relative FA (Fig. 3A) and T_2 (Fig. 3B) from the core and recovery ROIs of treated and control groups before and after TBI. There was no difference between T_2 and FA 2 days after TBI. The mean relative values of the core FA remained low (<1) within 6 weeks after TBI in both control and treated groups; however, the mean relative values of FA in the recovery ROIs gradually increased ($p < 0.01$ at 1–6 weeks) over a 6-week period in both groups (Fig. 3A). The treated group revealed large increases in FA in the recovery region soon after treatment compared with the control group, and differences were detected at 6 weeks after TBI ($p < 0.05$). There were no significant differences in core FA between treated and control groups.

T_2 exhibited a different temporal profile from FA (Fig. 3B). The mean relative T_2 values in both treated and control groups remained low or decreased in the recovery ROI, compared with the continuous increase in relative T_2 values in the core ROI, from 1 to 6 weeks after TBI. Differences between core and recovery ROIs in both treated and control groups were statistically significant ($p = 0.044$ at 2 weeks in the treated group and $p < 0.001$ at other time points 2–6 weeks in both the treated and control groups.). Core T_2 values were elevated significantly in controls compared with the treated group ($p < 0.01$ at 2 and 3 weeks and $p < 0.05$ at 4 and 6 weeks after TBI); however, there were no significant differences in the relative T_2 values in the recovery ROIs between treated and control groups.

The functional mNSS behavioral test was performed on both hMSC-treated and control rats at 1, 7, 14, 21, 28, 35 and 42 days after TBI. No significant difference was detected at 1 day (baseline) (Fig. 4A); however, there was a significant therapeutic effect on functional recovery at 3 ($p = 0.021$), 4 ($p = 0.017$), 5 ($p = 0.015$) and 6 weeks ($p < 0.001$) after TBI. The functional Morris water maze test revealed a significant therapeutic effect on functional recovery 39–42 days after TBI ($p < 0.001$) (Fig. 4B).

Visualization of white matter reorganization after MSC treatment

Figure 5 shows *in vivo* trace apparent diffusion coefficient (ADC) and FA maps from 2 days to 6 weeks after TBI in the same treated animal as shown in Fig. 1 (Fig. 5A), and corresponding *ex vivo* FA, radial ($\lambda_\perp$) and axial ($\lambda_{||}$) diffusivity, AKC, FT, Gaussian and *q*-ball fiber orientation direction (FD) maps (Fig. 5B), and Bielshowsky and Luxol fast blue images (Fig. 5C–G) from the fixed animal brain 6 weeks after TBI. White matter

reorganization after MSC treatment, confirmed by an increase in axons (C–G, black) and myelination (C–G, blue), coincided with increases in FA (Fig. 5B, FA; Fig. 5D, red arrowheads) in the extended region of the corpus callosum surrounding the lesion. The white matter reorganized regions corresponded well with the labeled cells shown in Fig. 1 and were separated by the lesion (Fig. 5B, arrowheads). The FA maps thus raised the question of how the separated areas of white matter were able to re-establish connectivity. The FT map derived from DTI (Fig. 5B, FT) revealed connections between the white matter reorganized regions separated by the TBI lesion (Fig. 5B, colored lines and arrowheads). These connections corresponded visually with the white matter reorganized region on the *ex vivo* coronal FA map (Fig. 5B, *ex vivo* coronal FA, arrow/arrowheads). The AKC map revealed increased AKC not only at the boundary of the lesion, as shown on the FA map, but also at the base of the lesion (yellow arrow), where fiber crossings of axons were confirmed by the *q*-ball fiber orientation map (Fig. 5B, yellow arrows) and the Bielshowsky and Luxol fast blue images (Fig. 5D, yellow arrowheads; Fig. 5F, arrowheads). The fiber orientation map derived from Gaussian DTI (Fig. 5B, Gaussian FD) did not provide any information about fiber crossings. The diffusivity maps gave complementary information; the white matter tracks exhibited decreased radial diffusivity (Fig. 5B, $\lambda_{\perp}$, arrowheads) and increased axial diffusivity (Fig. 5B, λ_2, arrowheads).

DISCUSSION

Using MRI, we investigated white matter reorganization after TBI with and without hMSC treatment, which was found to increase functional recovery and white matter reorganization, as reflected by increased FA. White matter reorganization was located primarily in the extended area of the corpus callosum and co-localized with labeled cells. The damaged corpus callosum re-established axonal connectivity along the boundary of the lesion, which can be monitored by DTI-based FT. Although FA showed promise, it could not detect early white matter reorganization with prominent crossing axons. Conversely, AKC was able to detect early axon reorganization. These novel results demonstrate that MRI can be used to dynamically investigate white matter reorganization.

We found that white matter became reorganized after TBI, especially in the extended area of the corpus callosum. TBI induces molecular and cellular changes at the boundary of the injury and in remote regions of the brain, including proliferation and differentiation of neural stem and progenitor cells, migration of neuroblasts to the boundary of the lesion and unmasking of previously inhibited connections (16,39–41). Axonal sprouting in the healthy brain is inhibited, a process controlled by myelin-associated proteins, extracellular matrix proteins and growth cone inhibitors. Injury induces axonal sprouting (16,40,42–44), new synaptic connections and myelination in both injured and neighboring regions (45). MSC treatment of ischemic damage increases significantly both progenitor and mature oligodendrocytes in the ipsilateral hemisphere (16). Oligodendrocytes generate myelin and contribute to the integrity of white matter tracts in the brain. The stimulation and amplification of these cells may lead to the restructuring of axons and myelin. White matter architecture at the boundary of the injury is altered by MSC treatment, and axonal density in the peri-infarct area is increased significantly in treated animals (13,16).

Although DTI has been applied to post-TBI injury (11,12), previous investigations have focused primarily on the detection of white matter damage rather than the effects of white matter reorganization on recovery. The current study demonstrates the ability of MRI to detect not only white matter damage, but also reorganization after MSC treatment. FA was able to monitor well-organized white matter recovery, and similar results have been described for the detection of white matter recovery after cell-based treatment of stroke (13). However, our data demonstrate that FA is unable to detect white matter reorganization when

the white matter fiber bundles cross. The inability of conventional DTI metrics to resolve multiple fiber directions derives from the assumption of Gaussian diffusion inherent to the diffusion tensor model (18–20). Conversely, DKI quantifies non-Gaussian water diffusion in tissue. AKC derived from DKI provides a quantitative means of assessing tissue microstructure, such as cellular compartments and membranes, and is more sensitive to axonal density than orientation. We determined that AKC is superior to FA in the detection of white matter reorganization with prominent crossing axons; moreover, it is sensitive to early stages of white matter reorganization (more crossing fibers) and increases significantly compared with the relatively low FA. However, both AKC and FA show a similar pattern if the white matter bundle is well organized in a single direction. A combination of AKC and FA may provide information about the stage of white matter reorganization in the injured brain: increased AKC in the absence of elevated FA would represent an early stage of recovery, as typified by random crossing fibers, whereas increased FA would identify more mature linear fibers.

Our data reveal that white matter reorganization is located primarily in the extended region of the corpus callosum and appears to promote cortical reorganization after TBI. The corpus callosum is the largest white matter structure in the mammalian brain and acts as a bridge connecting the two hemispheres. There is substantial evidence that injury-related lesions induce prolonged projections between hemispheres, as well as extending into the cortex (46,47). Our data show a marked increase in FA in the white matter extending from the corpus callosum to the boundary of the lesion, suggesting that hMSC treatment facilitates white matter changes involving the corpus callosum. In addition, DTI FT data show that the overall direction of axons at the boundary of the lesion is oriented differently from and rotates relative to the contralateral site in the normal brain, so that DTI can detect re-established connectivity around the lesion.

The anatomical basis for the increase in white matter changes and re-established connectivity is unknown; however, several factors may be involved. First, the white matter recovery region may undergo axonal sprouting, thereby forming new connections with other neurons in order to promote functional recovery, as observed in the extended region of the corpus callosum. Second, astrocytes may play an important role in changes in axonal orientation. The direction of axons may depend on the orientation of the reactive astrocytic fibers (48). Communication between neurons and glia is essential for axonal conduction, synaptic transmission and information processing, and is required for normal functioning of the nervous system during childhood and adolescence and throughout adult life (49). Astrocytes regulate the environment around neurons, including ion fluxes, neurotransmitters, cell adhesion molecules, specialized signaling molecules and a wide range of neuronal growth factors (49). By releasing neurotransmitters and other extracellular signaling molecules, astrocytes can affect neuronal excitability and synaptic transmission, and coordinate activity across networks of neurons (49). The secretion of neurotrophins from hMSCs (50) may promote a permissive local astrocytic biochemical microenvironment that supports axonal regeneration at the boundary of the lesion. Third, oligodendrocytes may play an important role in white matter reorganization. Cell-based treatment of ischemic damage increases significantly both progenitor and mature oligodendrocytes, as well as synaptic proteins, in the ipsilateral hemisphere of the ischemic brain (16,51). Oligodendrocytes generate myelin and contribute to the integrity of white matter tracks in the brain. The stimulation and amplification of these cells could lead to the restructuring of axons and myelin. White matter architecture at the ischemic boundary is altered by cell-based treatment, and axonal density in the peri-infarct area is reportedly increased significantly in treated animals (13,16,52). Fourth, a scar may form a wall around the lesion, preventing axons from entering the injured region and forcing them to re-establish new connections along the boundary. Indeed, our FT data showed that reorganized axons

changed orientation along the boundary of the lesion, and this was confirmed by immunohistological staining. Previous investigations have also shown that MSC treatment makes the scar wall thinner and reduces the number of microglia and macrophages within the wall (16). Although the relationship between axonal remodeling and the scar wall remains unclear, our data clearly demonstrate that DTI with FT algorithms can monitor noninvasively changes in orientation of white matter.

In our study, the labeled hMSC distribution corresponded to the region of white matter reorganization. One concern was that the detection of labeled hMSCs using Prussian blue staining could be confounded by the phagocytosis of iron particles by labeled microglia and macrophages; nevertheless, double staining with an antibody against human mitochondria and Prussian blue confirmed that most of the labeled cells detected were, indeed, hMSCs. Although we do not know how hMSCs affect white matter reorganization, functional recovery may be related to the activation of endogenous restorative mechanisms in the brain (53), rather than the replacement of dead neurons as originally proposed (54). MSCs are localized to the boundary of the lesion (3,4) and probably undergo complex cell–cell interactions, possibly similar to those that occur during embryonic development (55). MSCs survive in the injured brain and act as small molecular ‘factories’ that continue to secrete an array of trophic growth factors, including basic fibroblast growth factor, nerve growth factor, epidermal growth factor, transforming growth factor-β, vascular endothelial growth factor, insulin-like growth factor and brain-derived neurotrophic factor (3,4,56). More importantly, MSCs can stimulate neurotrophins and growth factors, including basic fibroblast growth factor, vascular endothelial growth factor and brain-derived neurotrophic factor, within parenchymal cells in response to injury (3,4,57). MSC-induced changes in trophic growth factors may affect the migration of neuroblasts, synaptogenesis and axonal reorganization, and thus promote functional recovery (3,4,57). In the current study, the most probable site of white matter recovery was the corpus callosum, where the labeled MSCs became aggregated and could have promoted white matter reorganization by the amplification of endogenous processes (16,17).

Our T_2 measurements provided complementary information that aided in the detection of white matter recovery. T_2 values remained lower in the recovery region than in the injured core. Elevated T_2 after TBI correlated with the severity of tissue damage and the development of edema (58–60). The relatively lower values of T_2 in the reorganized white matter may reflect enhanced recovery, whereas the decrease in T_2 in the core may reflect the effect of MSC treatment on edema. Measurements of the lesion volume on T_2 maps also showed a decrease as a result of treatment. Several studies have shown that effective treatment improves functional recovery without reducing lesion volume (51,61,62); however, our results are consistent with others showing reduced lesion volume and functional recovery after treatment (16,63). Although T_2 maps cannot identify reorganized white matter, they provide additional information that complements the FA and AKC data, and can help to characterize the status of tissue injury with and without white matter recovery.

CONCLUSIONS

Our data indicate that MRI can be used to identify white matter damage and recovery after TBI. FA, T_2 and AKC can evaluate white matter recovery following MSC treatment, which is evident in the extended region of the corpus callosum and co-localized with the labeled cells. Changes in AKC and FA in the reorganized white matter may provide information about the stage of white matter reorganization. Of these methods, AKC, FA and FT appear to be most useful for the identification of white matter recovery status, rewiring and location, and T_2 provides complementary information that can help to characterize tissue

injury related to edema. Our data suggest that AKC, FA and FT are important methodologies for potential application to the restorative therapy of patients with TBI.

Acknowledgments

This work was supported by National Institutes of Health (NIH) grants RO1 NS38292, RO1 NS43324, RO1 HL64766, PO1 NS23393, R01 AG027852 and PO1 NS42345.

Abbreviations used

ADC	apparent diffusion coefficient
AKC	apparent kurtosis coefficient
ANOVA	analysis of variance
DAI	diffuse axonal injury
DKI	diffusional kurtosis imaging
DSI	diffusion spectrum imaging
DTI	diffusion tensor MRI
FA	fractional anisotropy
FD	fiber orientation direction
FT	fiber tracking
HEPES	N-2-hydroxyethylpiperazine-N′-2-ethanesulfonic acid
hMSC	human bone marrow stromal cell
MEM	minimum essential medium
mNSS	modified neurological severity score
MSC	bone marrow stromal cell
ODF	orientation distribution function
PASMRI	persistent angular structure MRI
q-DTI	q-space DTI
ROI	region of interest
TBI	traumatic brain injury
$\lambda_{\perp}$	$\lambda_{\|\|}$, radial and axial diffusivity

References

1. Becker, DP.; Gade, GF.; Yound, HF.; Feuerman, TF. Diagnosis and treatment of head injury in adults. In: Youmans, JR., editor. Neurological Surgery. WB Saunders; Philadelphia, PA: 1990. p. 2017-2148.

2. Narayan RK, Michel ME, Ansell B, Baethmann A, Biegon A, Bracken MB, Bullock MR, Choi SC, Clifton GL, Contant CF, Coplin WM, Dietrich WD, Ghajar J, Grady SM, Grossman RG, Hall ED, Heetderks W, Hovda DA, Jallo J, Katz RL, Knoller N, Kochanek PM, Maas AI, Majde J, Marion DW, Marmarou A, Marshall LF, McIntosh TK, Miller E, Mohberg N, Muizelaar JP, Pitts LH, Quinn P, Riesenfeld G, Robertson CS, Strauss KI, Teasdale G, Temkin N, Tuma R, Wade C, Walker MD, Weinrich M, Whyte J, Wilberger J, Young AB, Yurkewicz L. Clinical trials in head injury. J Neurotrauma. 2002; 19(5):503–557. [PubMed: 12042091]

3. Li Y, Chopp M. Marrow stromal cell transplantation in stroke and traumatic brain injury. Neurosci Lett. 2009; 456(3):120–123. [PubMed: 19429146]
4. Xiong Y, Mahmood A, Chopp M. Emerging treatments for traumatic brain injury. Expert Opin Emerging Drugs. 2009; 14(1):67–84.
5. Dunnett SB, Bjorklund A, Lindvall O. Cell therapy in Parkinson's disease – stop or go? Nat Rev Neurosci. 2001; 2(5):365–369. [PubMed: 11331920]
6. Auerbach JM, Eiden MV, McKay RD. Transplanted CNS stem cells form functional synapses in vivo. Eur J Neurosci. 2000; 12(5):1696–1704. [PubMed: 10792447]
7. Zhang ZG, Jiang Q, Zhang R, Zhang L, Wang L, Arniego P, Ho KL, Chopp M. Magnetic resonance imaging and neurosphere therapy of stroke in rat. Ann Neurol. 2003; 53(2):259–263. [PubMed: 12557295]
8. Bulte JW, Zhang S, van Gelderen P, Herynek V, Jordan EK, Duncan ID, Frank JA. Neurotransplantation of magnetically labeled oligodendrocyte progenitors: magnetic resonance tracking of cell migration and myelination. Proc Natl Acad Sci USA. 1999; 96(26):15256–15261. [PubMed: 10611372]
9. Jiang Q, Zhang ZG, Ding GL, Zhang L, Ewing JR, Wang L, Zhang R, Li L, Lu M, Meng H, Arbab AS, Hu J, Li QJ, Pourabdollah Nejad DS, Athiraman H, Chopp M. Investigation of neural progenitor cell induced angiogenesis after embolic stroke in rat using MRI. Neuroimage. 2005; 28:697–698.
10. Gennarelli TA, Thibault LE, Adams JH, Graham DI, Thompson CJ, Marcincin RP. Diffuse axonal injury and traumatic coma in the primate. Ann Neurol. 1982; 12(6):564–574. [PubMed: 7159060]
11. Arfanakis K, Haughton VM, Carew JD, Rogers BP, Dempsey RJ, Meyer ME. Diffusion tensor MR imaging in diffuse axonal injury. Am J Neuroradiol. 2002; 23(5):794–802. [PubMed: 12006280]
12. Huisman TA, Schwamm LH, Schaefer PW, Koroshetz WJ, Shetty-Alva N, Ozsunar Y, Wu O, Sorensen AG. Diffusion tensor imaging as potential biomarker of white matter injury in diffuse axonal injury. Am J Neuroradiol. 2004; 25(3):370–376. [PubMed: 15037457]
13. Jiang Q, Zhang ZG, Ding GL, Silver B, Zhang L, Meng H, Lu M, Pourabdollah Nejad DS, Wang L, Savant-Bhonsale S, Li L, Bagher-Ebadian H, Hu J, Arbab AS, Vanguri P, Ewing JR, Ledbetter K, Chopp M. MRI detects white matter reorganization after neural progenitor cell treatment of stroke. Neuroimage. 2006; 32:1080–1089. [PubMed: 16860575]
14. Adams JH, Doyle D, Graham DI, Lawrence AE, McLellan DR. Microscopic diffuse axonal injury in cases of head injury. Med Sci Law. 1985; 25(4):265–269. [PubMed: 4068956]
15. Rugg-Gunn FJ, Symms MR, Barker GJ, Greenwood R, Duncan JS. Diffusion imaging shows abnormalities after blunt head trauma when conventional magnetic resonance imaging is normal. J Neurol Neurosurg Psychiatry. 2001; 70(4):530–533. [PubMed: 11254782]
16. Li Y, Chen J, Zhang CL, Wang L, Lu D, Katakowski M, Gao Q, Shen LH, Zhang J, Lu M, Chopp M. Gliosis and brain remodeling after treatment of stroke in rats with marrow stromal cells. Glia. 2005; 49(3):407–417. [PubMed: 15540231]
17. Shen LH, Li Y, Chen J, Zhang J, Vanguri P, Borneman J, Chopp M. Intracarotid transplantation of bone marrow stromal cells increases axon–myelin remodeling after stroke. Neuroscience. 2006; 137:393–399. [PubMed: 16298076]
18. Alexander DC, Barker GJ, Arridge SR. Detection and modeling of non-Gaussian apparent diffusion coefficient profiles in human brain data. Magn Reson Med. 2002; 48(2):331–340. [PubMed: 12210942]
19. Basser PJ, Pajevic S, Pierpaoli C, Duda J, Aldroubi A. In vivo fiber tractography using DT-MRI data. Magn Reson Med. 2000; 44(4):625–632. [PubMed: 11025519]
20. Tuch DS, Reese TG, Wiegell MR, Makris N, Belliveau JW, Wedeen VJ. High angular resolution diffusion imaging reveals intravoxel white matter fiber heterogeneity. Magn Reson Med. 2002; 48(4):577–582. [PubMed: 12353272]
21. Wedeen VJ, Hagmann P, Tseng WY, Reese TG, Weisskoff RM. Mapping complex tissue architecture with diffusion spectrum magnetic resonance imaging. Magn Reson Med. 2005; 54(6): 1377–1386. [PubMed: 16247738]
22. Tuch DS, Reese TG, Wiegell MR, Wedeen VJ. Diffusion MRI of complex neural architecture. Neuron. 2003; 40(5):885–895. [PubMed: 14659088]

23. Alexander DC. Multiple-fiber reconstruction algorithms for diffusion MRI. Ann NY Acad Sci. 2005; 1064:113–133. [PubMed: 16394152]
24. Tuch DS. Q-ball imaging. Magn Reson Med. 2004; 52(6):1358–1372. [PubMed: 15562495]
25. Jensen, JH.; Helpern, JA. Quantifying non-Gaussian water diffusion by means of pulsed-field-gradient MRI. The Proceedings of 11th International Society for Magnetic Resonance in Medicine; Toronto, Canada. 2003. p. 2154
26. Jensen JH, Helpern JA, Ramani A, Lu H, Kaczynski K. Diffusional kurtosis imaging: the quantification of non-gaussian water diffusion by means of magnetic resonance imaging. Magn Reson Med. 2005; 53(6):1432–1440. [PubMed: 15906300]
27. Lazar M, Jensen JH, Xuan L, Helpern JA. Estimation of the orientation distribution function from diffusional kurtosis imaging. Magn Reson Med. 2008; 60(4):774–781. [PubMed: 18816827]
28. Cheung MM, Hui ES, Chan KC, Helpern JA, Qi L, Wu EX. Does diffusion kurtosis imaging lead to better neural tissue characterization? A rodent brain maturation study. Neuroimage. 2009; 45(2): 386–392. [PubMed: 19150655]
29. Dixon CE, Clifton GL, Lighthall JW, Yaghmai AA, Hayes RL. A controlled cortical impact model of traumatic brain injury in the rat. J Neurosci Methods. 1991; 39(3):253–262. [PubMed: 1787745]
30. Lu D, Mahmood A, Wang L, Li Y, Lu M, Chopp M. Adult bone marrow stromal cells administered intravenously to rats after traumatic brain injury migrate into brain and improve neurological outcome. Neuroreport. 2001; 12(3):559–563. [PubMed: 11234763]
31. Lu D, Mahmood A, Qu C, Hong X, Kaplan D, Chopp M. Collagen scaffolds populated with human marrow stromal cells reduce lesion volume and improve functional outcome after traumatic brain injury. Neurosurgery. 2007; 61(3):596–602. discussion 602–603. [PubMed: 17881974]
32. Xiong Y, Qu C, Mahmood A, Liu Z, Ning R, Li Y, Kaplan DL, Schallert T, Chopp M. Delayed transplantation of human marrow stromal cell-seeded scaffolds increases transcallosal neural fiber length, angio-genesis, and hippocampal neuronal survival and improves functional outcome after traumatic brain injury in rats. Brain Res. 2009; 1263:183–191. [PubMed: 19368838]
33. von Bohlenund, Halbach O, Albrecht D. Tracing of axonal connectivities in a combined slice preparation of rat brains – a study by rhodamine-dextran-amine-application in the lateral nucleus of the amygdala. J Neurosci Methods. 1998; 81(1–2):169–175. [PubMed: 9696322]
34. Salthouse TN. Luxol fast blue G as a myelin stain. Stain Technol. 1964; 39:123. [PubMed: 14127797]
35. Chen J, Li Y, Wang L, Zhang Z, Lu D, Lu M, Chopp M. Therapeutic benefit of intravenous administration of bone marrow stromal cells after cerebral ischemia in rats. Stroke. 2001; 32(4): 1005–1011. [PubMed: 11283404]
36. Lu D, Goussev A, Chen J, Pannu P, Li Y, Mahmood A, Chopp M. Atorvastatin reduces neurological deficit and increases synaptogenesis, angiogenesis, and neuronal survival in rats subjected to traumatic brain injury. J Neurotrauma. 2004; 21(1):21–32. [PubMed: 14987462]
37. Mori S, van Zijl PC. Fiber tracking: principles and strategies – a technical review. NMR Biomed. 2002; 15(7–8):468–480. [PubMed: 12489096]
38. Alexander DC, Barker GJ. Optimal imaging parameters for fiber-orientation estimation in diffusion MRI. Neuroimage. 2005; 27(2):357–367. [PubMed: 15921931]
39. Zhang ZG, Chopp M. Neurorestorative therapies for stroke: underlying mechanisms and translation to the clinic. Lancet Neurol. 2009; 8(5):491–500. [PubMed: 19375666]
40. Nudo RJ. Mechanisms for recovery of motor function following cortical damage. Curr Opin Neurobiol. 2006; 16(6):638–644. [PubMed: 17084614]
41. Cramer SC, Shah R, Juranek J, Crafton KR, Le V. Activity in the peri-infarct rim in relation to recovery from stroke. Stroke. 2006; 37(1):111–115. [PubMed: 16306462]
42. Aldskogius H, Kozlova EN. Central neuron–glial and glial–glial interactions following axon injury. Prog Neurobiol. 1998; 55(1):1–26. [PubMed: 9602498]
43. Fok-Seang J, DiProspero NA, Meiners S, Muir E, Fawcett JW. Cytokine-induced changes in the ability of astrocytes to support migration of oligodendrocyte precursors and axon growth. Eur J Neurosci. 1998; 10(7):2400–2415. [PubMed: 9749768]
44. Dancause N, Barbay S, Frost SB, Plautz EJ, Chen D, Zoubina EV, Stowe AM, Nudo RJ. Extensive cortical rewiring after brain injury. J Neurosci. 2005; 25(44):10167–10179. [PubMed: 16267224]

45. Tanaka K, Nogawa S, Suzuki S, Dembo T, Kosakai A. Upregulation of oligodendrocyte progenitor cells associated with restoration of mature oligodendrocytes and myelination in peri-infarct area in the rat brain. Brain Res. 2003; 989(2):172–179. [PubMed: 14556938]
46. Carmichael ST, Chesselet MF. Synchronous neuronal activity is a signal for axonal sprouting after cortical lesions in the adult. J Neurosci. 2002; 22(14):6062–6070. [PubMed: 12122067]
47. Napieralski JA, Butler AK, Chesselet MF. Anatomical and functional evidence for lesion-specific sprouting of corticostriatal input in the adult rat. J Comp Neurol. 1996; 373(4):484–497. [PubMed: 8889940]
48. Imaizumi T, Lankford KL, Kocsis JD, Hashi K. The role of transplanted astrocytes for the regeneration of CNS axons. No To Shinkei. 2001; 53(7):632–638. [PubMed: 11517487]
49. Fields RD, Stevens-Graham B. New insights into neuron–glia communication. Science. 2002; 298(5593):556–562. [PubMed: 12386325]
50. Labouyrie E, Dubus P, Groppi A, Mahon FX, Ferrer J, Parrens M, Reiffers J, de Mascarel A, Merlio JP. Expression of neurotrophins and their receptors in human bone marrow. Am J Pathol. 1999; 154(2):405–415. [PubMed: 10027399]
51. Liu Z, Li Y, Qu R, Shen L, Gao Q, Zhang X, Lu M, Savant-Bhonsale S, Borneman J, Chopp M. Axonal sprouting into the denervated spinal cord and synaptic and postsynaptic protein expression in the spinal cord after transplantation of bone marrow stromal cell in stroke rats. Brain Res. 2007; 1149:172–180. [PubMed: 17362881]
52. Liu Z, Li Y, Zhang X, Savant-Bhonsale S, Chopp M. Contralesional axonal remodeling of the corticospinal system in adult rats after stroke and bone marrow stromal cell treatment. Stroke. 2008; 39(9):2571–2577. [PubMed: 18617661]
53. Chopp M, Li Y. Treatment of neural injury with marrow stromal cells. The Lancet Neurol. 2002; 1:92–100.
54. McKay R. Stem cells in the central nervous system. Science. 1997; 276(5309):66–71. [PubMed: 9082987]
55. Prockop DJ, Azizi SA, Colter D, Digirolamo C, Kopen G, Phinney DG. Potential use of stem cells from bone marrow to repair the extra-cellular matrix and the central nervous system. Biochem Soc Trans. 2000; 28(4):341–345. [PubMed: 10961915]
56. Phinney DG, Hill K, Michelson C, DuTreil M, Hughes C, Humphries S, Wilkinson R, Baddoo M, Bayly E. Biological activities encoded by the murine mesenchymal stem cell transcriptome provide a basis for their developmental potential and broad therapeutic efficacy. Stem Cells. 2006; 24(1):186–198. [PubMed: 16100003]
57. Lu D, Mahmood A, Chopp M. Biologic transplantation and neurotrophin-induced neuroplasticity after traumatic brain injury. J Head Trauma Rehabil. 2003; 18(4):357–376. [PubMed: 16222130]
58. Jiang Q, Chopp M, Zhang ZG, Knight RA, Jacobs M, Windham JP, Peck D, Ewing JR, Welch KM. The temporal evolution of MRI tissue signatures after transient middle cerebral artery occlusion in rat. J Neurol Sci. 1997; 145(1):15–23. [PubMed: 9073024]
59. Jiang Q, Zhang RL, Zhang ZG, Knight RA, Ewing JR, Ding G, Lu M, Arniego P, Zhang L, Hu J, Li Q, Chopp M. Magnetic resonance imaging characterization of hemorrhagic transformation of embolic stroke in the rat. J Cereb Blood Flow Metab. 2002; 22(5):559–568. [PubMed: 11973428]
60. Jiang Q, Ewing JR, Zhang ZG, Zhang RL, Hu J, Divine GW, Arniego P, Li QJ, Chopp M. Magnetization transfer MRI: application to treatment of middle cerebral artery occlusion in rat. J Magn Reson Imaging. 2001; 13(2):178–184. [PubMed: 11169822]
61. Shen LH, Li Y, Chen J, Cui Y, Zhang C, Kapke A, Lu M, Savant-Bhonsale S, Chopp M. One-year follow-up after bone marrow stromal cell treatment in middle-aged female rats with stroke. Stroke. 2007; 38(7):2150–2156. [PubMed: 17525391]
62. Shen LH, Li Y, Chen J, Zacharek A, Gao Q, Kapke A, Lu M, Raginski K, Vanguri P, Smith A, Chopp M. Therapeutic benefit of bone marrow stromal cells administered 1 month after stroke. J Cereb Blood Flow Metab. 2007; 27(1):6–13. [PubMed: 16596121]
63. Li L, Jiang Q, Zhang L, Ding G, Wang L, Zhang R, Zhang ZG, Li Q, Ewing JR, Kapke A, Lu M, Chopp M. Ischemic cerebral tissue response to subventricular zone cell transplantation measured by iterative self-organizing data analysis technique algorithm. J Cereb Blood Flow Metab. 2006; 26(11):1366–1377. [PubMed: 16511501]

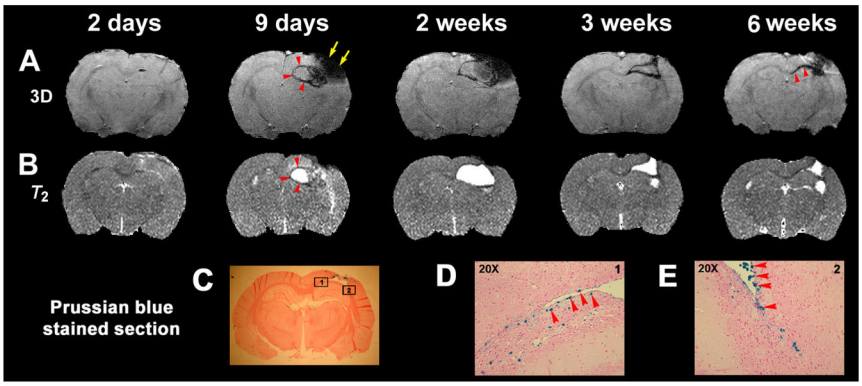

Figure 1.

Labeled cell migration and distribution after bone marrow stromal cell (MSC) treatment of traumatic brain injury (TBI). (A, B) Three-dimensional MRI (A) and T_2 (B) maps from 2 days (5 days before labeled MSC injection) to 6 weeks after TBI. (C–E) Prussian blue-stained sections (D and E from the boxes in C) obtained from the same rat 6 weeks after TBI, showing clusters of blue cells around the boundary of the lesion and the corpus callosum (D, E, blue cells, red arrowheads), as demonstrated by three-dimensional MRI (A, 6 weeks, red arrowheads).

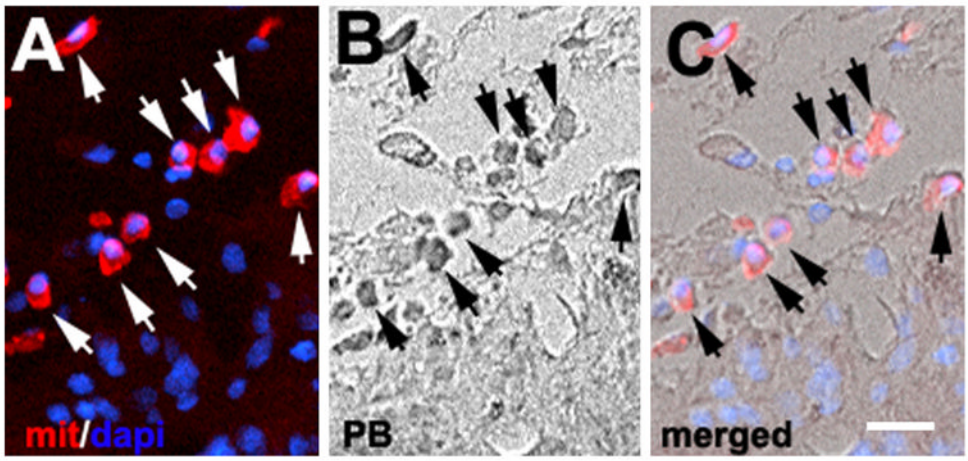

Figure 2.

Identification of labeled human bone marrow stromal cells (hMSCs). Immunofluorescent staining shows human mitochondrial cells (A, red, arrows) positive for Prussian blue (PB) (B, arrows). (C) Merging of (A) and (B). Nuclei were stained with 4′,6-diamidino-2-phenylindole (dapi) (blue). Bar, 20 μm.

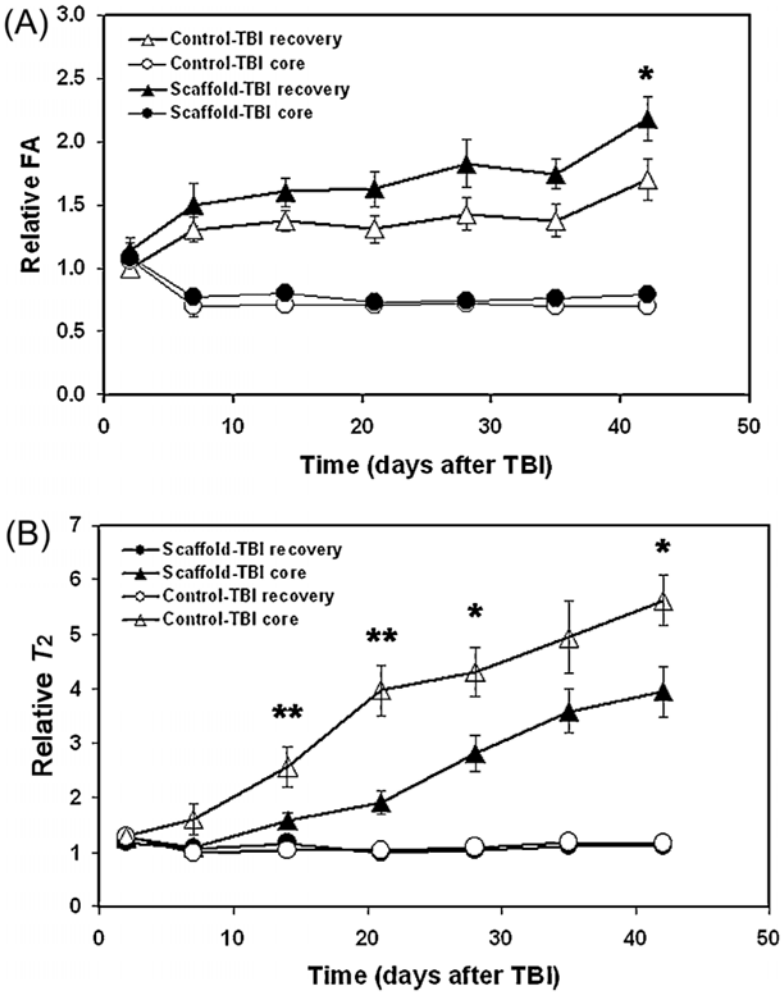

Figure 3.

(A, B) Quantitative characterization of MRI parameters in traumatic brain injury (TBI)-damaged tissue with and without human bone marrow stromal cell (hMSC) treatment. The graphs show the evolution of changes in fractional anisotropy (FA) and T_2 with and without scaffold + hMSC treatment of TBI. Significant differences were detected in FA (p <0.05 at 6 weeks in the recovery region) and T_2 (p < 0.01 at 2 and 3 weeks and p <0.05 at 4 and 6 weeks in the core region) between treated and nontreated groups. $^{*}p$ <0.05 and $^{**}p$ <0.01 comparing treated and nontreated groups.

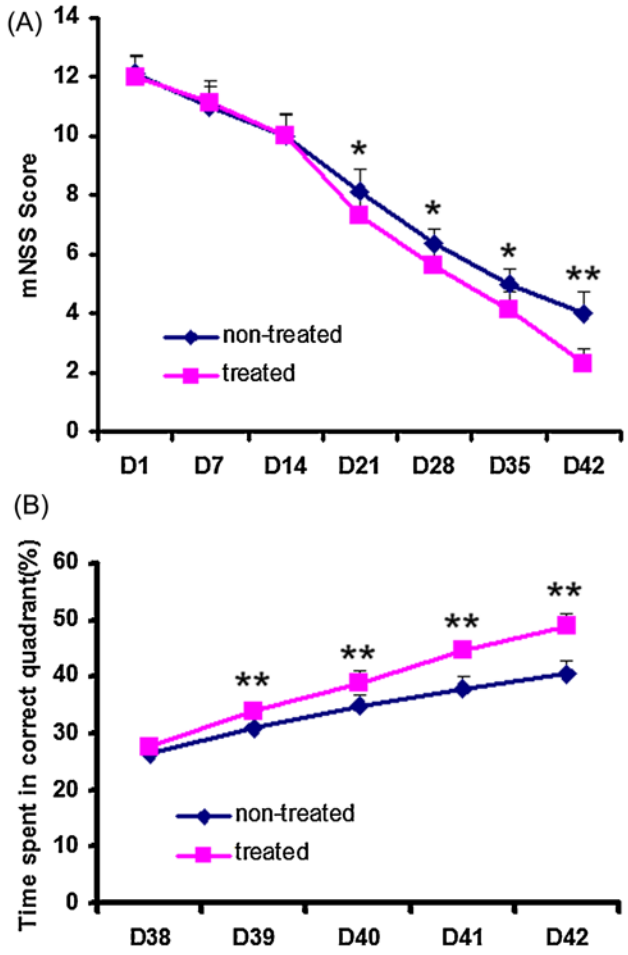

Figure 4.

Functional recovery after bone marrow stromal cell (MSC) treatment of traumatic brain injury (TBI). The graphs show the functional improvement as detected with the modified neurological severity score (mNSS, A) and modified Morris water maze test (B). $^{*}p < 0.05$ and $^{**}p < 0.01$ comparing treated and nontreated groups.

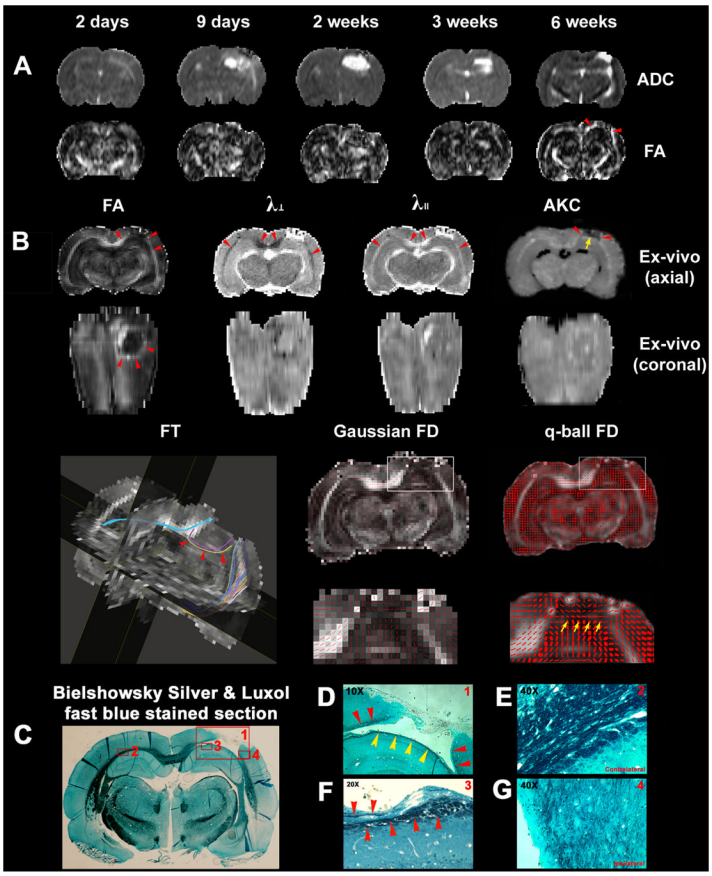

Figure 5.

MRI detection of white matter remodeling after bone marrow stromal cell (MSC) treatment of traumatic brain injury (TBI). Evolution of *in vivo* trace apparent diffusion coefficient (ADC) and fractional anisotropy (FA) maps (A), corresponding *ex vivo* FA, radial ($\lambda_{\perp}$) and axial ($\lambda_{\parallel}$) diffusivity, apparent kurtosis coefficient (AKC), fiber tracking, Gaussian and *q*-ball fiber orientation maps (B), and Bielshowsky and Luxol fast blue immunoreactive staining images (C–G) measured in the fixed animal brain. (D–G) High-magnification images from the areas shown in the box in (C) as indicated in the top right-hand corners of (D)–(G).